Addition of Oxygen to the Diiron(II/II) Cluster Is the Slowest Step in Formation of the Tyrosyl Radical in the W103Y Variant of Ribonucleotide Reductase Protein R2 from Mouse†

Danny Yun,‡,§ Lana Saleh,‡,|| Ricardo García-Serres,⊥ Brandon M. Chicalese,‡ Young H. An,‡ Boi Hanh Huynh,⊥ and J. Martin Bollinger, Jr.*,‡

Departments of Biochemistry and Molecular Biology and of Chemistry, The Pennsylvania State University, University Park, Pennsylvania 16802, and Department of Physics, Emory University, Atlanta, Georgia 30322

Received February 22, 2007; Revised Manuscript Received August 11, 2007

ABSTRACT: Activation of O_2 by the diiron(II/II) cluster in protein R2 of class I ribonucleotide reductase generates the enzyme's essential tyrosyl radical. A crucial step in this reaction is the transfer of an electron from solution to a diiron(II/II)−O_2 adduct during formation of the radical-generating, diiron(III/IV) intermediate **X**. In the reaction of R2 from *Escherichia coli*, this electron injection is initiated by the rapid (>400 s^{-1} at 5 °C), transient oxidation of the near-surface residue, tryptophan 48, to a cation radical and is blocked by substitution of W48 with F, A, G, Y, L, or Q. By contrast, a study of the cognate reaction in protein R2 from mouse suggested that electron injection might be the slowest step in generation of its tyrosyl radical, Y177• [Schmidt, P. P., Rova, U., Katterle, B., Thelander, L., and Gräslund, A. (1998) *J. Biol. Chem. 273*, 21463−21472]. The crucial evidence was the observation that Y177• production is slowed by ∼30-fold upon substitution of W103, the cognate of the electron-shuttling W48 in *E. coli* R2, with tyrosine. In this work, we have applied stopped-flow absorption and freeze-quench electron paramagnetic resonance and Mössbauer spectroscopies to the mouse R2 reaction to evaluate the possibility that an already sluggish electron-transfer step is slowed by 30-fold by substitution of this key residue. The drastically reduced accumulation of cluster **X**, failure of precursors to the intermediate to accumulate, and, most importantly, first-order dependence of the rate of Y177• formation on the concentration of O_2 prove that addition of O_2 to the diiron(II/II) cluster, rather than electron injection, is the slowest step in the R2-W103Y reaction. This finding indicates that the basis for the slowing of Y177• formation by the W103Y substitution is an unexpected secondary effect on the structure or dynamics of the protein, its diiron(II/II) cluster, or both rather than the expected chemical effect on the electron injection step.

Among the diiron carboxylate oxidase and oxygenase proteins (a family that includes, among others, soluble methane monooxygenase, toluene 4-monooxygenase, and stearoyl acyl carrier protein Δ^9-desaturase), protein R2 of class I ribonucleotide reductase (RNR[1]) is unique in its "splitting" of the two oxidizing equivalents of the initial adduct between O_2 and the diiron(II/II) center to generate a one-electron-oxidized product, the stable tyrosyl radical that is necessary for the protein's catalytic activity in the RNR holoenzyme (R1·R2) complex (*1*−*5*). The step that permits this unique outcome is the transfer of an electron from an exogenous reductant to the buried active site after addition of O_2 to the diiron(II/II) cluster (*6*−*9*). In the most extensively studied R2 protein, that from *Escherichia coli*, this electron injection proceeds in two steps: transient oxidation of the near-surface tryptophan residue W48 to a cation radical ($W48^{\bullet+}$) and subsequent reduction of $W48^{\bullet+}$ from solution (*10*−*12*). Electron donation by W48 is sufficiently rapid to prevent accumulation of the diiron complex that oxidizes the residue. As a result, $W48^{\bullet+}$ forms along with the tyrosyl-radical-generating diiron(III/IV) cluster **X** in a kinetically second-order reaction between the Fe(II)−R2 complex and O_2 (*11*, *13*). Substitution of W48 with other residues disables rapid electron injection and results in the direct generation of the Y122 radical together with **X** by the same intermediate (presumably) that oxidizes W48 in the reaction of the wild-type protein (*12*). Y122• is generated 10-fold more rapidly by this altered mechanism than by **X** in the R2-wt reaction and is unstable due to the inability of the W48-substituted variant protein to mediate reduction of the adjacent **X**. Consequently, **X** and Y122• decay together

† This work was supported by NIH Grants GM55365 to J.M.B. and GM58778 to B.H.H.

* To whom correspondence should be addressed. Phone: (814) 863-5707. Fax: (814) 863-7024. E-mail: jmb21@psu.edu.

‡ The Pennsylvania State University.

§ Present address: Department of Chemistry, Massachusetts Institute of Technology, Cambridge, MA 02139.

|| Present address: New England Biolabs, 240 County Rd., Ipswich, MA 01938.

⊥ Emory University.

[1] Abbreviations: RNR, ribonucleotide reductase; EPR, electron paramagnetic resonance; k_{obsd}, observed apparent first-order rate constant; Y177•, tyrosyl radical in mouse R2; Y122•, tyrosyl radical in *E. coli* R2; IPTG, isopropyl thiogalactopyranoside; PMSF, phenylmethanesulfonyl fluoride; Tris, tris(hydroxymethyl)aminomethane; HEPES, 4-[2-hydroxyethyl]-1-piperazineethanesulfonic acid; PCR, polymerase chain reaction; SDS−PAGE, sodium dodecyl sulfate−polyacrylamide gel electrophoresis.

10.1021/bi7003747 CCC: $37.00
Published on Web 10/17/2007

by an unknown mechanism to yield primarily nonradical products (*12*, *14*). Y122• can be rescued from decay in the R2-W48F reaction by inclusion of the potent reductant dithionite (*12*) and in the R2-W48A reaction by inclusion of analogues of the truncated indole side chain (e.g., 3-methylindole) (*14*).

An early investigation of the cofactor assembly reaction in protein R2 from mouse (*Mus musculus*) suggested that it might differ markedly in kinetic details or even more profoundly in mechanistic pathway from the *E. coli* R2 reaction (*15*). Most notably, the authors proposed that electron injection is the slowest step in this reaction and presented a mechanism in which an intermediate more oxidized than the product diiron(III/III) cluster by two electrons [i.e., a diiron(IV/IV) complex] might accumulate to high levels. The latter proposal suggested that the mouse R2 reaction might afford the opportunity for characterization of an intermediate that is not detectable in the *E. coli* R2 reaction. The crucial observations in support of the Schmidt et al. hypothesis and mechanism were (1) the failure of a kinetically competent cognate of cluster **X** to accumulate and (2) the slowing (by 20−30-fold) of Y177• formation in the reactions of variants with W103 or D266, the cognates of W48 and its hydrogen-bonding partner D237 in *E. coli* R2, substituted by Y or A, respectively. A later study contradicted the first conclusion, showing accumulation of cluster **X** and its kinetic competence as the Y177•-generating complex (*16*), but was unable definitively to rationalize the discrepancy with the earlier study.

In this study, the kinetics and mechanism of O_2 activation and Y177• formation in mouse R2-W103Y have been reexamined both to reevaluate the second crucial piece of evidence for slow electron injection in the mouse R2 reaction and to explore the basis for the very different behaviors of mouse R2-W103Y (slower formation of stable Y177•) and *E. coli* R2-W48X variants (faster formation of transient Y122•). Evidence obtained by stopped-flow absorption and freeze-quench Mössbauer and EPR kinetic experiments establishes that the primary effect of this substitution, slowing of Y177• formation, results not from the expected effect on the electron injection step but from an unanticipated retardation of addition of O_2 to the diiron(II/II) cluster. This finding provides an explanation for one primary difference between the behaviors of W48- and W103-substituted variants of the *E. coli* and mouse R2 proteins and, together with the previous studies of the wild-type protein (*16*, *17*), consolidates our understanding of tyrosyl radical generation in class I RNRs in general.

MATERIALS AND METHODS

Materials. Culture medium components (yeast extract and tryptone) were purchased from Marcor Development Corp. (Hackensack, NJ). Isopropyl β-D-thiogalactopyranoside (IPTG) was purchased from Biosynth International (Naperville, IL). Spectinomycin dihydrochloride, phenylmethylsulfonyl fluoride (PMSF), streptomycin sulfate, Trizma base (Tris), and 1,10-phenanthroline were purchased from Sigma (St. Louis, MO). Ampicillin was purchased from IBI (Shelton, CT). Glycerol, ammonium sulfate, and sodium chloride were purchased from EM Science (Gibbstown, NJ). Enzyme-grade 4-(2-hydroxyethyl)-1-piperazineethanesulfonic acid (HEPES) was purchased from FisherBiotech (Pittsburgh, PA). Oligonucleotide primers were purchased from Gibco/BRL (Grand Island, NY). Restriction enzymes and reagents for the polymerase chain reaction (PCR) were purchased from New England Biolabs (Beverly, MA). T4 DNA ligase was purchased from Roche (Indianapolis, IN). DNA sequence determination was performed by the Nucleic Acid Facility of The Pennsylvania State University Biotechnology Institute. BL21(DE3) and pET vectors were purchased from Novagen (Madison, WI). The plasmid pSJS1240 (*18*) was a kind gift from Professor Craig Cameron (The Pennsylvania State University).

Preparation of the Plasmid Vector for Overexpression of R2-W103Y in E. coli. The W103Y substitution was introduced by using the polymerase chain reaction (PCR) and the previously described plasmid pMR2, which contains the mouse R2 gene inserted into the pET22b expression vector (*16*). Primers 1 (5′-GGA GAT ATA **CAT ATG** CTC TCC GTC CGC-3′, *Nde*I site shown in bold) and 2 (5′-CCA AAA **GCT AGC** CTC GGC TTT CTT GTA CAT CTG CC-3′, *Nhe*I site shown in bold) were used to amplify a 323-base-pair fragment (1) and introduce an *Nhe*I restriction site, which is 5′ of the W103 codon. Fragment 1 was purified by agarose gel electrophoresis, extracted from the gel by using the Qiagen (Valencia, CA) QiaQuick system as instructed by the manufacturer, restricted with *Nde*I and *Nhe*I, and repurified. The second gene fragment encoding the W103 to Y substitution (TGG to TAT, italic) was created by using primers 3 (5′-GCC GAG **GCT AGC** TTT *TAT* ACT GCC GAG GAG GTG G-3′, *Nhe*I site shown in bold) and 4 (5′-GTT AGC AGC **CTC GAG** TTA GAA GTC AGC ATC CAA GG-3′, *Xho*I site shown in bold). This 893-base-pair fragment was gel purified, restricted with *Nhe*I and *Xho*I, repurified, and ligated with fragment 1 and pET22b, which had been restricted with *Nde*I and *Xho*I and gel purified. The sequence of the entire coding region was verified. BL21-(DE3) cells were transformed with the pMR2-W103Y and pSJS1240 plasmids.

Purification of Apo-R2-W103Y. BL21(DE3) cells containing the pMR2-W103Y and pSJS1240 plasmids were grown, and apo-R2-W103Y was expressed as previously described (*16*). The apo form of R2-W103Y was purified as previously described for the wild-type protein (*16*, *17*).

Determination of Protein Concentration. The molar absorptivity, ϵ_{280}, assumed for the R2-W103Y dimer is 115 180 M^{-1} cm^{-1}. This value was determined by subtraction of 5690 M^{-1} cm^{-1} ($\times 2$), the ϵ_{280} of a tryptophan residue (*19*), from the molar absorptivity of 124 000 M^{-1} cm^{-1} reported for the mouse R2 dimer (*20*) and addition of 1280 M^{-1} cm^{-1} ($\times 2$), the ϵ_{280} of a tyrosine residue (*19*), to the resulting value.

Kinetic Experiments. The apparatus and procedures employed for the stopped-flow absorption and freeze-quench EPR and Mössbauer experiments have been described (*16*, *21*, *22*). Details of the reaction and spectrometer conditions are given in the appropriate figure captions.

RESULTS

Expression and Purification of R2-W103Y. Expression of R2-W103Y in BL21(DE3)-pMR2-W103Y and purification (primarily) by anion exchange chromatography (*16*) yielded preparations that, like those of the wild-type protein, exhibit

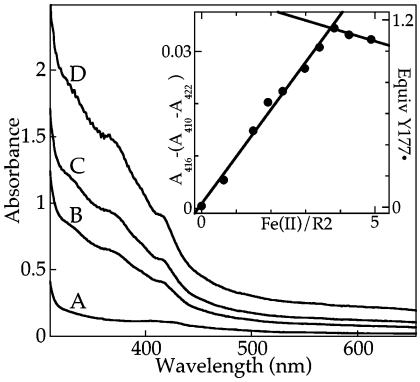

FIGURE 1: Spectrophotometrically monitored titration of apo-R2-W103Y with Fe(II) in the presence of O_2. The titration was carried out in the presence of 2.5 mM sodium ascorbate as previously described (*16*). The spectra shown were acquired after addition of (A) 0, (B) 1.5, (C) 2.3, and (D) 3.8 equiv of Fe(II) relative to R2 dimer (concentration of 0.12 mM). The inset shows plots of $A_{416} - (A_{410} + A_{422})/2$ and equivalents of Y177• versus equivalents of Fe(II) added.

a triplet band pattern in SDS−PAGE analysis that is indicative of partial proteolysis (data not shown). The effects of the proteolysis on the O_2 reaction are not known. However, given that identical proteolysis was also observed in all previous investigations of the mouse R2 reaction (*20*, *23*), results from the different studies can be directly compared.

Determination of Limiting Fe(II)/R2-W103Y, Y177•/R2-W103Y, and Fe(II)/Y177• Stoichiometries for the Reaction. The quality of the preparations was assessed by titration in the presence of O_2 with Fe(II) to determine the number of functional diiron sites per R2-W103Y dimer and the yield of the tyrosine Y177 radical (Y177•). Upon addition of Fe(II) to the apoprotein, absorption bands characteristic of the (μ-oxo)diiron(III/III) cluster (~365 nm) and Y177• (416 nm) develop in seconds (Figure 1). The Fe(II)/R2 ratio necessary to reach maximal levels of Y177•, as monitored by the height of the peak at 416 nm [$A_{416} - (A_{410} - A_{422})/2$; *16*] through the titration, implies that apo-R2-W103Y can take up 3.3−3.8 equiv of Fe(II) (inset to Figure 1). Comparison of the 416 nm peak height to the [Y177•] determined directly by quantitative EPR analysis of similar samples (see Figure S1 of the Supporting Information) (*8*) reveals that Y177• has an effective molar absorptivity in R2-W103Y of 247 ± 20 M^{-1} cm^{-1} on the standard spectrophotometer used to acquire the spectra of Figure 1 and 180 ± 15 M^{-1} cm^{-1} on the diode array spectrophotometer associated with the stopped-flow apparatus. The variant protein supports formation of somewhat less Y177• (1.0 ± 0.2 equiv) than the wild-type protein (1.6 ± 0.2 equiv). This observation is consistent with those reported by other investigators (*15*, *24*).

Kinetics of Y177• Production in Reaction of Fe(II)−R2-W103Y with O_2. The kinetics of Y177• formation upon mixing of the preformed Fe(II)−R2-W103Y complex with O_2 at 5 °C were examined in stopped-flow absorption experiments. The height of the peak at 416 nm [given by $A_{416} - (A_{410} + A_{422})/2$] can be used to resolve the kinetics of Y177•, as described in our previous studies (*16*, *17*). Multiple phases of Y177• formation are observed (Figure 2, blue symbols). The apparent first-order rate constant for the fastest phase estimated by regression "fitting" (see below for more rigorous simulation analysis) is 0.8 (±0.2) s^{-1} at an O_2 concentration of 0.9 mM. This value is ~6-fold less

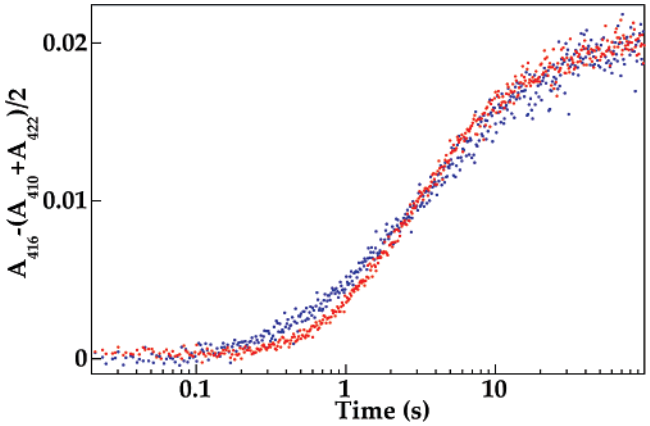

FIGURE 2: Kinetics of tyrosyl radical formation in mouse R2-W103Y at 5 °C after equal-volume mixing either of an O_2-free solution [in 100 mM HEPES, pH 7.6, 10% (v/v) glycerol (buffer A)] containing 0.34 mM R2-W103Y and 1.2 mM Fe(II) (3.5 equiv) with an O_2-saturated solution of buffer A (blue data points) or of an O_2-free solution of 0.34 mM apo-R2-W103Y in buffer A with an O_2-saturated solution of 1.2 mM Fe(II) (3.5 equiv) in 2.5 mM H_2SO_4 (red data points). The reaction was monitored by stopped-flow absorption spectroscopy, and the traces show $A_{416} - (A_{410} + A_{422})/2$ as a function of time. In both cases, the final [O_2] should have been 0.95 mM. The path length in both experiments was 1 cm.

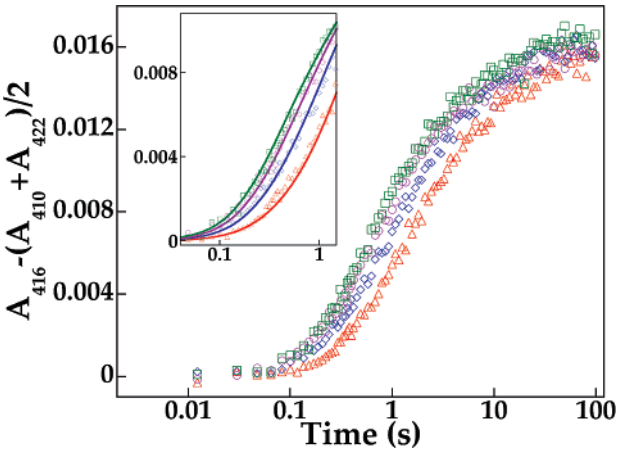

FIGURE 3: Dependence of the kinetics of Y177• formation on [O_2] in the reaction of Fe(II)−R2-W103Y with excess O_2 at 10 °C. An O_2-free solution of 0.33 mM apo-R2-W103Y and 1.4 mM Fe(II) (4 equiv) in buffer B (100 mM HEPES, pH 7.6, 24% (w/w) glycerol) was mixed with 2.5 equivalent volumes of buffer B containing varying [O_2]. The desired [O_2] in the buffer solutions was achieved by mixing O_2-saturated buffer with O_2-free buffer in appropriate ratios. The estimated [O_2] after mixing was 0.32 mM (red triangles), 0.64 mM (blue tilted squares), 1.0 mM (purple circles), and 1.3 mM (green squares). The inset shows a blowup of the first 1.5 s of the reaction to emphasize the key observation that the rate of the initial fast phase of Y177• production depends on [O_2]. The solid lines in the inset are simulations according to Scheme 1.

than that for Y177• production in the reaction of wild-type R2 (5 ± 2 s^{-1}), in qualitative agreement with the report by Schmidt et al. that the W103Y substitution slows Y177• formation (*15*).

Kinetics of Y177• Production in the Reaction of Apo-R2-W103Y with Fe(II) and O_2. Complex (multiphasic) kinetics were also observed in the reaction of the Fe(II) complex of wild-type R2 with O_2 (*16*, *17*). In that case, the faster phase of Y177• formation was attributed to reaction of the preformed Fe(II)−R2 complex with O_2 and the slower phase

Scheme 1: Scheme Used in Simulation of the Kinetic Data from the Reaction of Fe(II)−R2-W103Y with O_2 at 10 °C

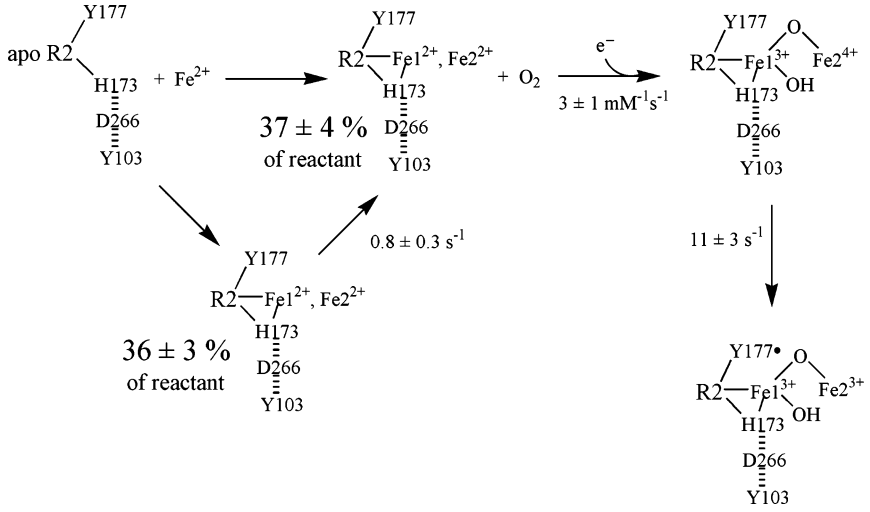

to the relatively slow uptake of Fe(II) by apo-R2 remaining in the reactant solution followed by reaction of the complex with O_2. The basis for this attribution was the observation that only the slow phase is observed when the apoprotein is mixed in the presence of O_2 with Fe(II) (i.e., when the complex is not allowed to form prior to initiation of the reaction). Stopped-flow experiments, in which O_2-containing solutions of apo-R2-W103Y and Fe(II) were mixed, were carried out to test whether the same explanation might apply for the complex kinetics in the reaction of the variant protein. By contrast to the situation with the wild-type protein, Y177• formation is only slightly less rapid when initiated in this manner (red symbols in Figure 2) and is still multiphasic. Thus, the much slower phase(s) of Y177• production observed in the reaction of the Fe(II)−R2-W103Y complex with O_2 cannot be due to slow uptake of Fe(II) by a fraction of protein remaining in the apo form. A detectable lag phase (with an apparent first-order rate constant of $\sim$10 s^{-1}), which is not present in the reaction of the preformed complex with O_2, is observed in the apoprotein versus Fe(II) + O_2 reaction (compare red and blue symbols in Figure 2). This lag phase most likely reflects formation of the reactive Fe(II)−R2-W103Y complex prior to O_2 activation. This conclusion would imply that formation of the reactive complex is slightly faster for the variant protein than for R2-wt (k_{obsd} = 0.29 ± 0.03) and, unlike for the wild-type protein, is not the slowest step in Y177• formation.

Dependence of the Kinetics of Y177• Production on [O_2]. To probe the nature of the slowest step, stopped-flow absorption experiments were carried out with varying concentrations of O_2. The fastest phase of Y177• production is dependent on the concentration of O_2, whereas the slower phases are independent of [O_2] (Figure 3). Kinetic simulations based on Scheme 1 reproduce the [O_2] dependence of the fastest phase (Figure 3, inset). The observation of a first-order dependence of the kinetics of formation of the final product (Y177•) on the concentration of the reactant O_2 has important implications for the identity of the slowest step in the reaction, as discussed below.

*Kinetics of the Reaction and Detection of **X** by Freeze-Quench EPR Spectroscopy.* The [O_2] dependence implies that intermediates between the reactants and the product Y177• do not accumulate to high levels. If an intermediate were to accumulate, a lag phase in product formation would be observed, and the duration of the lag would respond to changes in [O_2]. The subsequent formation of the product would be less dependent on (or, in the limit of stoichiometric accumulation of the intermediate, completely independent of) [O_2]. To test more directly for accumulation of intermediates, the reaction was monitored by the freeze-quench EPR and Mössbauer methods. X-band EPR spectra at 20 K of samples freeze-quenched through the course of the reaction reveal increasing intensity attributable to Y177• (Figure 4). The spectra of samples frozen at reaction times between 0.017 and 0.15 s have somewhat different line shapes (spectra A, B, and C), revealing the presence of another g = 2.00 signal. These spectra can be reproduced well by summation of the spectra of **X** and Y177• with appropriate weighting factors (spectra A′, B′, and C′). These reconstructions allow the concentration of **X** and Y177• in each sample to be calculated from the weighting factors and the total integrated intensity, as previously described (*16*, *17*). The kinetics of Y177• so deduced (filled purple squares in Figure 5) agree almost precisely with those obtained from the stopped-flow absorption experiments with the most similar reaction conditions (open purple squares). The kinetics of **X** (filled blue squares) provide constraints for modeling of the fast phase of the reaction according to Scheme 1 (solid lines in Figure 5). Importantly, the rate constants for the addition of O_2 to produce **X** and decay of **X** to produce Y177• that are necessary to accommodate the minimal accumulation of the intermediate are consistent with the [O_2] dependence of formation of Y177• observed in stopped-flow absorption experiments.

Kinetics of the Reaction by Freeze-Quench Mössbauer Spectroscopy. In Scheme 1, reaction of Fe(II)−R2-W103Y with O_2 is assumed to lead directly to **X** in a single step. This assumption implies that intervening states [e.g., the peroxodiiron(III/III) complex demonstrated in ref *17*] do not accumulate and thus need not be considered in a minimal kinetic mechanism. To verify this crucial prediction, the reaction was probed by the freeze-quench Mössbauer method. An O_2-free solution of Fe(II)−R2-W103Y (3.8 equiv of Fe(II)/R2) was rapidly mixed with O_2-saturated buffer, and Mössbauer samples were prepared by freeze-quenching at reaction times of 0.013, 0.060, 0.22, 0.6, and 4 s. Repre-

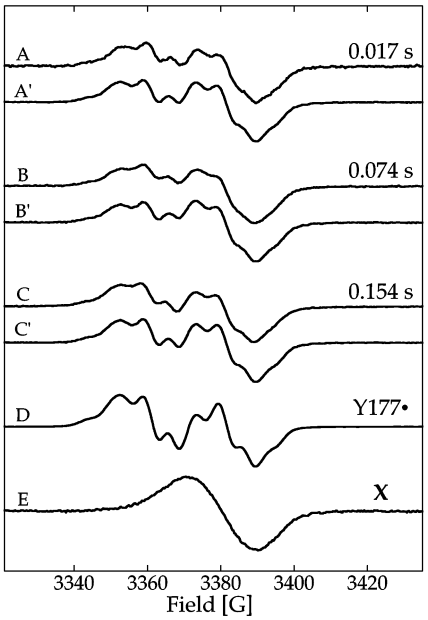

FIGURE 4: Component analysis of EPR spectra of samples obtained by mixing an O_2-free solution of 0.87 mM mouse R2-W103Y and 3.0 mM Fe(II) (3.5 equiv) in buffer B (see the Figure 3 caption) with 2 equivalent volumes of an O_2-saturated solution of buffer B. In each of the first three pairs of spectra, the upper spectrum (labeled A, B, or C) is of the sample freeze-quenched at the indicated reaction time, and the lower spectrum (labeled A′, B′, or C′) is the corresponding reconstruction by summation of the reference spectra for Y177• (spectrum D) and **X** (spectrum E). Spectrum D is of the 100 s sample. Spectrum E is of a sample obtained as previously described (*16*). All spectra were recorded at 20 K with a microwave power of 6.3 μW and a modulation amplitude of 4 G. For spectra A−D, a scan time of 160 s and a time constant of 0.16 s were used. For spectrum E, the scan time was increased to 1300 s and the time constant to 1.3 s. Integrated spectral intensities were related to concentration by use of a copper perchlorate standard, as previously described (*8*).

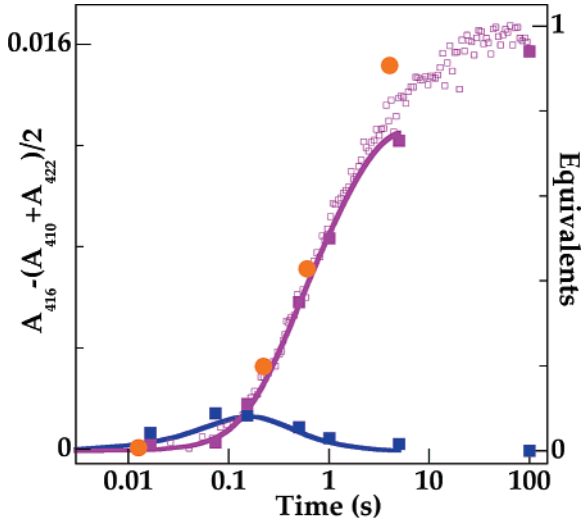

FIGURE 5: Kinetics of formation and decay of **X** (blue squares) and formation of Y177• (open purple squares for stopped-flow absorption and filled purple squares for EPR) and the (μ-oxo)diiron(III/III) cluster (filled orange circles) in the reaction of Fe(II)−R2-W103Y [3.5−4.0 equiv of Fe(II)] with excess O_2. The filled symbols are from freeze-quench experiments, and the open symbols are from the stopped-flow absorption experiments. The stopped-flow data are from the experiment of Figure 3 with 1.4 mM O_2. The freeze-quench EPR experiment (for **X** and Y177•) and freeze-quench Mössbauer experiment [for the (μ-oxo)diiron(III/III) cluster] are described in the captions to Figures 4 and 6, respectively. The solid lines are from simulations according to Scheme 1 and the concentrations of the freeze-quench EPR experiment (Figure 4).

sentative spectra are shown in Figure 6. The data confirm that intermediate complexes barely accumulate. The quadrupole doublet of the reactant Fe(II) species (solid green lines; see the Figure 6 caption for parameters) decays monotonically as the pair of partially resolved doublets of the (μ-oxo)diiron(III/III) product (solid orange lines) develop. The magnetically split spectrum of **X** (see, for example, ref *17* for this spectrum) is not observable in the spectra shown in Figure 6 and is barely detectable (with imagination) in the spectrum of the 0.22 s sample (data not shown). An upper bound of 5% absorption intensity relative to the total Fe absorption was estimated for **X** in the 0.22 s sample, consistent with the very low level of accumulation (<0.1 equiv) deduced by EPR. The kinetics of formation of the (μ-oxo)diiron(III/III) product obtained by analysis of these spectra (filled orange circles in Figure 5) agree well with those for Y177• deduced by stopped-flow absorption and EPR. Additional features that develop nearly in parallel with those of the normal (μ-oxo)diiron(III/III) product are well-modeled as two quadrupole doublets (solid red lines in Figure 6) with the parameters shown in the caption to Figure 6. These features arise from an additional stable product that forms in competition with the normal (μ-oxo)diiron(III/III) product cluster. Altered products were previously observed in the reaction of the cognate variant of *E. coli* R2, R2-W48F (*12*). Importantly, the time-dependent Mössbauer spectra show that decay of the Fe(II) species and formation of the normal product have similar, surprisingly sluggish kinetics.

DISCUSSION

The dependence of the kinetics of Y177• formation on [O_2], the meager accumulation of the Y177•-generating complex **X**, and the failure of precursors to **X** to accumulate establish that the slowest step in O_2 activation by Fe(II)−R2-W103Y involves conversion of the reactants to **X**. Two distinct kinetic scenarios could accommodate the data. First and most simply, addition of O_2 to the diiron(II/II) cluster of the reactant complex may be slow. Second, O_2 addition may be fast, reversible, and very disfavored at the accessible reactant concentrations. In this case, very little of the initial diiron(II/II)−O_2 complex would accumulate, and the reaction would be limited by forward conversion of the initial complex to **X**. The latter scenario is potentially consistent, at least in part, with the hypothesis of Schmidt et al. that electron transfer is slow (*15*): conversion of the initial complex to **X** would involve and could be rate-limited by the electron-transfer step. However, the results of a recent study (*17*) provide a compelling argument against this second scenario. This study showed that a peroxodiiron(III/III) complex similar to that characterized in variants of *E. coli* R2 with the D84E ligand substitution accumulates to a relatively high level (~0.4 equiv) in the reaction of the Fe(II) complex of wild-type mouse R2 with O_2. This complex precedes electron transfer in the mechanistic sequence. Its formation is not obviously reversible and is clearly not as disfavored under these conditions as would be required to rationalize the kinetic data for the R2-W103Y reaction by a kinetic mechanism involving a slow electron-transfer step.

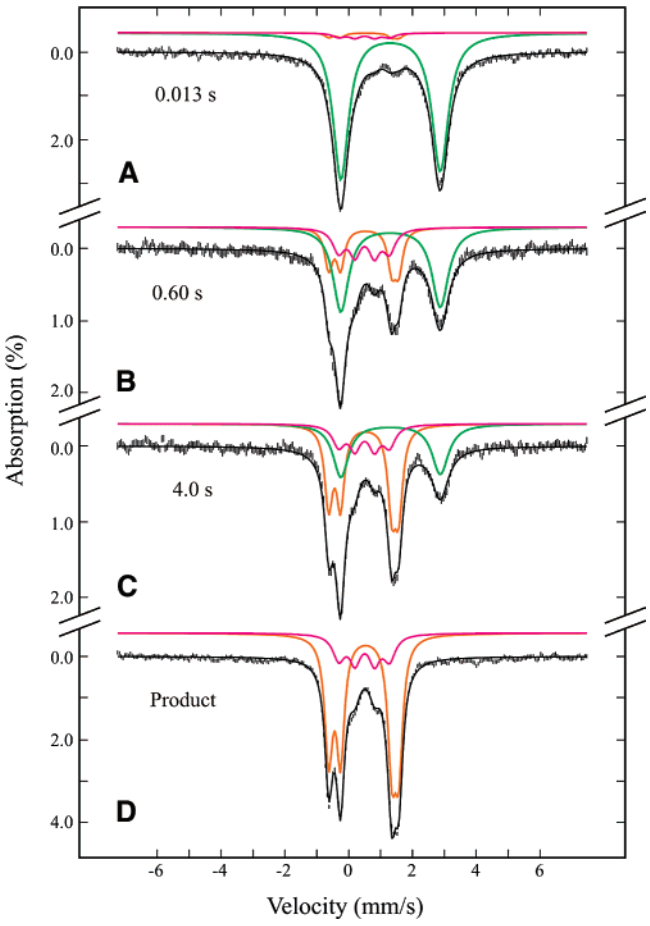

FIGURE 6: Mössbauer spectra at 4.2 K and 50 mT (parallel to the γ-beam) of freeze-quenched samples from the reaction of Fe(II)−R2-W103Y with excess O_2. An O_2-free solution of 0.99 mM R2-W103Y and 3.8 mM Fe(II) in buffer B was mixed at 10 °C with 2 equivalent volumes of O_2-saturated buffer B (see the Figure 3 caption). The reaction was quenched (A) 0.013 s, (B) 0.60 s, (C) 4 s, and (D) ~600 s after mixing. The colored solid lines plotted above the data are reference spectra of Fe(II)−R2 (green; $\delta = 1.31$ mm/s, $\Delta E_Q = 3.12$ mm/s, $\gamma_l = 0.587$ mm/s, $\gamma_r = 0.626$ mm/s), the (μ-oxo)diiron(III/III) cluster (orange; $\delta = 0.55$, 0.47 mm/s, $\Delta E_Q = 1.61$, 2.20 mm/s, $\gamma_l = 0.3$, 0.3 mm/s, $\gamma_r = 0.3$, 0.3 mm/s), and the altered product (red; $\delta = 0.48$, 0.50 mm/s, $\Delta E_Q = 1.59$, 0.61 mm/s, $\gamma_l = 0.45$, 0.41 mm/s, $\gamma_r = 0.45$, 0.41 mm/s). They are plotted at the following intensities of the total absorption area in (A), (B), (C), and (D), respectively: green, 89%, 51%, 32%, and 0%; orange, 3%, 25%, 50%, and 76%; red, 5%, 22%, 20%, and 24%. The solid black lines in (A)−(D) are summations of the reference spectra at these percentages.

Thus, the observations and analysis strongly disfavor the notion of slow electron transfer advanced by Schmidt et al. (*15*).

The data are completely and more simply accommodated by the conclusion that the slowest step in the reaction is the addition of O_2 to the diiron(II/II) cluster. The corollary to this conclusion would be that the W103Y substitution either retards protein dynamics that are required to allow O_2 to access the diiron site or influences the conformation of the diiron(II/II) cluster, disfavoring the reactive form in its rapid equilibrium with other, unreactive forms. In either case, the general conclusion would be the same: that the primary effect of the substitution relates not to the removal of chemical functionality necessary for the reaction (i.e., mediation of electron transfer) but to an unanticipated secondary structural or dynamical perturbation that slows a step in which W103 has no obvious chemical role. This conclusion implies, in turn, that the reaction of mouse R2 reaction differs from the cognate reaction in *E. coli* R2 only in relatively subtle kinetic details rather than more fundamentally in chemical mechanism.

SUPPORTING INFORMATION AVAILABLE

Table with the complete component analysis from the freeze-quench EPR experiment of Figure 4, figure showing the determination of the drop-line-corrected molar absorptivity [$\epsilon_{416} - (\epsilon_{410} + \epsilon_{422})/2$] of Y177• in mouse R2-W103Y, and figure showing residual errors of the simulations in the inset to Figure 3. This material is available free of charge via the Internet at http://pubs.acs.org.

REFERENCES

1. Nordlund, P., and Eklund, H. (1995) Di-iron-carboxylate proteins, *Curr. Opin. Struct. Biol. 5*, 758−766.
2. Wallar, B. J., and Lipscomb, J. D. (1996) Dioxygen activation by enzymes containing binuclear non-heme iron clusters, *Chem. Rev. 96*, 2625−2657.
3. Solomon, E. I., Brunold, T. C., Davis, M. I., Kemsley, J. N., Lee, S.-K., Lehnert, N., Neese, F., Skulan, A. J., Yang, Y.-S., and Zhou, J. (2000) Geometric and electronic structure/function correlations in non-heme iron enzymes, *Chem. Rev. 100*, 235−349.
4. Stubbe, J. (2003) Di-iron-tyrosyl radical ribonucleotide reductases, *Curr. Opin. Chem. Biol. 7*, 183−188.
5. Bollinger, J. M., Jr., and Krebs, C. (2006) Stalking intermediates in oxygen activation by iron enzymes: Motivation and method, *J. Inorg. Biochem. 100*, 586−605.
6. Ochiai, E., Mann, G. J., Gräslund, A., and Thelander, L. (1990) Tyrosyl free radical formation in the small subunit of mouse ribonucleotide reductase, *J. Biol. Chem. 265*, 15758−15761.
7. Bollinger, J. M., Jr., Edmondson, D. E., Huynh, B. H., Filley, J., Norton, J. R., and Stubbe, J. (1991) Mechanism of assembly of the tyrosyl radical-dinuclear iron cluster cofactor of ribonucleotide reductase, *Science 253*, 292−298.
8. Bollinger, J. M., Jr., Tong, W. H., Ravi, N., Huynh, B. H., Edmondson, D. E., and Stubbe, J. (1994) Mechanism of assembly of the tyrosyl-diiron(III) cofactor of *E. coli* ribonucleotide reductase. 2. Kinetics of the excess Fe^{2+} reaction by optical, EPR, and Mössbauer spectroscopies, *J. Am. Chem. Soc. 116*, 8015−8023.
9. Parkin, S. E., Chen, S., Ley, B. A., Mangravite, L., Edmondson, D. E., Huynh, B. H., and Bollinger, J. M., Jr. (1998) Electron injection through a specific pathway determines the outcome of oxygen activation at the diiron cluster in the F208Y mutant of *Escherichia coli* ribonucleotide reductase protein R2, *Biochemistry 37*, 1124−1130.
10. Bollinger, J. M., Jr., Tong, W. H., Ravi, N., Huynh, B. H., Edmondson, D. E., and Stubbe, J. (1994) Mechanism of assembly of the tyrosyl radical-diiron(III) cofactor of *E. coli* ribonucleotide reductase. 3. Kinetics of the limiting Fe^{2+} reaction of optical, EPR, and Mössbauer spectroscopies, *J. Am. Chem. Soc. 116*, 8024−8032.
11. Baldwin, J., Krebs, C., Ley, B. A., Edmondson, D. E., Huynh, B. H., and Bollinger, J. M., Jr. (2000) Mechanism of rapid electron transfer during oxygen activation in the R2 subunit of *Escherichia coli* ribonucleotide reductase. 1. Evidence for a transient tryptophan radical, *J. Am. Chem. Soc. 122*, 12195−12206.
12. Krebs, C., Chen, S., Baldwin, J., Ley, B. A., Patel, U., Edmondson, D. E., Huynh, B. H., and Bollinger, J. M., Jr. (2000) Mechanism of rapid electron transfer during oxygen activation in the R2 subunit of *Escherichia coli* ribonucleotide reductase. 2. Evidence for and consequences of blocked electron transfer in the W48F variant, *J. Am. Chem. Soc. 122*, 12207−12219.
13. Saleh, L., and Bollinger, J. M., Jr. (2006) Cation mediation of radical transfer between Trp48 and Tyr356 during O_2 activation by protein R2 of *Escherichia coli* ribonucleotide reductase: Relevance to R1−R2 radical transfer in nucleotide reduction?, *Biochemistry 45*, 8823−8830.
14. Saleh, L., Kelch, B. A., Pathickal, B. A., Baldwin, J., Ley, B. A., and Bollinger, J. M., Jr. (2004) Mediation by indole analogues of

electron transfer during oxygen activation in variants of *Escherichia coli* ribonucleotide reductase R2 lacking the electron-shuttling tryptophan 48, *Biochemistry 43*, 5943−5952.

15. Schmidt, P. P., Rova, U., Katterle, B., Thelander, L., and Gräslund, A. (1998) Kinetic evidence that a radical transfer pathway in protein R2 of mouse ribonucleotide reductase is involved in generation of the tyrosyl free radical, *J. Biol. Chem. 273*, 21463−21472.
16. Yun, D., Krebs, C., Gupta, G. P., Iwig, D. F., Huynh, B. H., and Bollinger, J. M., Jr. (2002) Facile electron transfer during formation of cluster **X** and kinetic competence of **X** for tyrosyl radical production in protein R2 of ribonucleotide reductase from mouse, *Biochemistry 41*, 981−990.
17. Yun, D., García-Serres, R., Chicalese, B. M., An, Y. H., Huynh, B. H., and Bollinger, J. M., Jr. (2007) (μ-1,2-Peroxo)diiron(III/III) complex as a precursor to the diiron(III/IV) intermediate, **X**, in the assembly of the iron-radical cofactor of ribonucleotide reductase from mouse, *Biochemistry 46*, 1925−1932.
18. Kim, R., Sandler, S. J., Goldman, S., Yokota, H., Clark, A. J., and Kim, S. H. (1998) Overexpression of archaeal proteins in *Escherichia coli*, *Biotechnol. Lett. 20*, 207−210.
19. Gill, S. C., and von Hippel, P. H. (1989) Calculation of protein extinction coefficients from amino acid sequence data, *Anal. Biochem. 182*, 319−326.
20. Mann, G. J., Graslund, A., Ochiai, E., Ingemarson, R., and Thelander, L. (1991) Purification and characterization of recombinant mouse and herpes simplex virus ribonucleotide reductase R2 subunit, *Biochemistry 30*, 1939−1947.
21. Bollinger, J. M., Jr., Tong, W. H., Ravi, N., Huynh, B. H., Edmondson, D. E., and Stubbe, J. (1995) Use of rapid kinetics methods to study the assembly of the diferric-tyrosyl radical cofactor of *E. coli* ribonucleotide reductase, *Methods Enzymol. 258*, 278−303.
22. Ravi, N., Bollinger, J. M., Jr., Huynh, B. H., Edmondson, D. E., and Stubbe, J. (1994) Mechanism of assembly of the tyrosyl radical-diiron(III) cofactor of *E. coli* ribonucleotide reductase: 1. Mössbauer characterization of the diferric radical precursor, *J. Am. Chem. Soc. 116*, 8007−8014.
23. Rova, U., Adrait, A., Pötsch, S., Gräslund, A., and Thelander, L. (1999) Evidence by mutagenesis that Tyr(370) of the mouse ribonucleotide reductase R2 protein is the connecting link in the intersubunit radical transfer pathway, *J. Biol. Chem. 274*, 23746−23751.
24. Rova, U., Goodtzova, K., Ingemarson, R., Behravan, G., Gräslund, A., and Thelander, L. (1995) Evidence by site-directed mutagenesis supports long-range electron transfer in mouse ribonucleotide reductase, *Biochemistry 34*, 4267−4275.

BI7003747